Montmorillonite-Filled Nanocomposites of Tung Oil/Styrene/Divinylbenzene Polymers Prepared by Thermal Polymerization

P. P. Kundu,[1] R. C. Larock[2]

[1]*Department of Polymer Science and Technology, University of Calcutta, 92 Acharyya Prafulla Chandra Road, Kolkata 700009, India*
[2]*Department of Chemistry, Iowa State University, Ames, Iowa 50011*

Received 19 January 2009; accepted 27 June 2009
DOI 10.1002/app.31046
Published online 18 August 2010 in Wiley Online Library (wileyonlinelibrary.com).

ABSTRACT: Montmorillonite-filled nanocomposites were prepared by the thermal copolymerization of tung oil (TUNG), styrene (ST), and divinylbenzene (DVB). These nanocomposites were characterized by X-ray diffraction (XRD), transmission electron microscopy (TEM), dynamic mechanical analysis (DMA), and their mechanical properties. The XRD of the modified montmorillonite exhibited a peak that vanished completely in the nanocomposites. Thus, the XRD results apparently indicate a distortion of the platy layers of the nanofiller in the TUNG–ST–DVB polymers. A platy nanolayered structure of the modified montmorillonite in the TUNG–ST–DVB polymers was observed by TEM. The extent of separation of the platy layers as observed by the TEM reached a maximum for the 5% modified nanofiller (at a fixed polymer composition), 50%-oil-containing polymer (at a fixed nanofiller concentration of 5%), and TUNG intragallery nanocomposites (at both fixed polymer and nanofiller concentrations). The DMA results show a broadened glass-transition temperature along with a hump for these nanofilled polymers, indicating the presence as a majority constituent of a copolymer consisting of TUNG and aromatics, along with a grafted TUNG polymer, respectively. The improvements in the Young's modulus and compressive strength upon incorporation of the nanofiller indicated the presence of a partially intercalated and distorted platy-layered structure of the nanofiller. However, from the results of all of these studies, it was tough to estimate the exact level of delamination/exfoliation in these TUNG nanocomoposites. © 2010 Wiley Periodicals, Inc. J Appl Polym Sci 119: 1297–1306, 2011

Key words: biomaterials; composites; crosslinking; mechanical properties; nanocomposites

INTRODUCTION

The definition of a nanocomposite material has broadened significantly to encompass a large variety of systems, indicating one-dimensional, two-dimensional, three-dimensional, and amorphous materials made of distinctly dissimilar components and mixed on a nanometer scale.[1–3] The general class of nanocomposite organic/inorganic materials is a fast-growing area of research. Significant recent effort has been focused on the ability to obtain control of the nanoscale structures via innovative synthetic approaches. The properties of nanocomposite materials depend not only on the properties of their individual components but also on their morphology and interfacial characteristics.

The inorganic components can be three-dimensional framework systems, such as zeolites;[4] two-dimensional layered materials, such as clays,[5] metal oxides,[6] and metal phosphates;[7] and even one-dimensional and zero-dimensional materials, such as $(Mo_3Se_3—)_n$ chains and clusters.[8] Experimental work has shown that virtually all types and classes of nanocomposite materials lead to new and improved properties when they are compared to their macrocomposite counterparts. Therefore, nanocomposites promise new applications in many fields, including mechanically reinforced lightweight components,[9] nonlinear optics,[10] battery cathodes,[11] ionics,[12] nanowires,[13] sensors,[14] and other systems. The general class of organic/inorganic nanocomposites may also be of relevance to issues of bioceramics and biomineralization in which *in situ* growth and polymerization of the biopolymer and inorganic matrix occurs.[15]

Common clays are naturally occurring minerals and are thus subject to natural variability in their constitution. The purity of a clay can affect the final nanocomposite properties. Many clays are aluminosilicates, which have a sheetlike (layered) structure and consist of silica (SiO_4) tetrahedra bonded to alumina (AlO_6) octahedra in a variety of ways. A 2:1 ratio of the tetrahedra to the octahedra results in

Correspondence to: P. P. Kundu (pp923@yahoo.com).

smectite clays, the most common of which is montmorillonite.[16–21] A necessary prerequisite for the successful formation of polymer–clay nanocomposites is, therefore, the alteration of the clay polarity to make the clay organophilic. An organophilic clay can be produced from a normally hydrophilic clay by ion exchange with an organic cation, such as an alkyl ammonium ion.[22]

The extremely large surface area and high aspect ratio (between 30 and 2000) of montmorillonite clay make property improvements possible; these result in the formation of a nanocomposite.[23–25] Among the vast nanoreinforcements available for fabricating polymer nanocomposites, researchers have focused on and studied clays the most because they are naturally occurring minerals, exhibit a layered morphology with high aspect ratios, and have substantial cation exchange capacities.[23–25] Montmorillonite is one filler, and many nanocomposites have been made from it, for instance, polyamide/montmorillonite,[26] epoxy/montmorillonite,[27] unsaturated polyester/montmorillonite,[28] polystyrene/montmorillonite,[29] and polypropylene/montmorillonite.[30]

It was reported that transparent thermosetting plastics can be made from tung oil (TUNG), styrene (ST), and divinylbenzene (DVB) by thermal polymerization.[31] In this study, we aimed to develop novel nanocomposites of these thermosets via *in situ* polymerization.

EXPERIMENTAL

Materials

The TUNG used in this study (supplied by Alnor Oil Co, Valley Stream, NY) was light yellow in color, and its principal constituent (~84%) was α-elaeostearic acid, that is, *cis*-9-, *trans*-11-, *trans*-13-octadecatrienoic acid, a conjugated triene. Montmorillonite (K-10), cetyl trimethyl ammonium bromide (CTAB), 1-hexadecyl amine (a precursor for the preparation of hexdecylammonium bromide), ST, and DVB (80 mol % DVB and 20 mol % ethylvinylbenzene), purchased from Aldrich Chemical Co. (Milwaukee, MI), were used as received.

Modification of the montmorillonite

We dispersed the montmorillonite clay in deionized water by stirring. CTAB or hexadecyl ammonium bromide (HDAB) was added to the dispersion. The whole dispersion was heated at 80°C for 4 h. The exchanged clays were filtered and washed with deionized water until they were free from bromide (tested and titrated by silver nitrate). The modified clay was dried at 80°C *in vacuo*. The cation-exchange capacities calculated from the titer value for CTAB and HDAB were 29.92 and 152.84 mequiv/100 g of clay, respectively.

TABLE I
Polymer Compositions and Modified Nanofiller Concentrations for the Preparation of the Nanolayered Composites

Entry	TUNG	ST	DVB	Modified nanofiller (CTABMONT)
S1	50	20	30	0
S2	50	20	30	2.5
S3	50	20	30	5.0
S4	50	20	30	7.5
S5	50	20	30	10.0
S6	30	28	42	5.0
S7	40	24	36	5.0
S8	60	16	24	5.0
S9	70	12	18	5.0
S10	—	40	60	2.5
S11	100	—	—	2.5
S12	50	20	30	2.5 (HDABMONT)
S13	50	20	30	2.5 (aromatic intragallery)
S14	50	20	30	2.5 (tung intragallery)
S15	50	20	30	2.5 (without stirring)
S16	50	20	30	2.5 (without modification but with stirring)
S17	50	20	30	2.5 (without modification or stirring)

Nanocomposite preparation

We prepared the polymeric nanocomposites by heating the desired mixture of TUNG, ST, DVB, and modified montmorillonite in a glass vial. The modified nanofillers of a predetermined quantity were dispersed in TUNG–ST–DVB at a fixed ratio of 50:20:30. The detailed compositions are shown in Table I. The dispersion was maintained by constant magnetic stirring at 500 rpm (overnight for proper intercalation). The mixture was heated at 85°C for 2 h and then at 120°C for 1–4 h, such that the viscosity of the liquid (prepolymer) was sufficiently high because of the formation of sufficient crosslinks, and the fillers should have been exfoliated. Under these conditions, the fillers did not separate from the prepolymer, even when stirring was stopped. The whole mass was transferred to an appropriate mold and put in a heated oven at 120°C for 2 h, 140°C for 24 h, and finally, 160°C for 24 h. We prepared the TUNG intragallery nanocomposites by stirring the nanofiller dispersion in the TUNG; we then heated the mixture at 120°C for 12 h. This led to *in situ* polymerization of the TUNG, which caused it to initiate exfoliation of the layered silicate. Then, the desired amount of ST and DVB were added to the mixture. On achieving the desired viscosity of the prepolymer by heating at 120°C for approximately 8 h, it was heated in an oven at 140°C for

24 h and then at 160°C for 24 h. We also prepared the aromatic intragallery nanocomposites in a similar manner by stirring the nanofiller dispersion in the appropriate mixture of ST and DVB and then heating the mixture at 80°C for a few hours to achieve the desired viscosity. Thus, the nanofiller was exfoliated during the *in situ* polymerization and crosslinking of the ST. At this point, an appropriate amount of TUNG was added to the mixture; it was then heated in an oven at 140°C for 24 h and then at 160°C for 24 h. All of the prepared nanocomposites were transparent and light yellow in color.

Characterization

Wide-angle X-ray diffraction (WAXRD)

Scanning intensity curves for values of 2θ ranging from 1.5 to 25° were determined by X-ray diffraction (XRD) analysis (XDS 2000, Scintag, Inc., Cupertino, CA) with powder polymeric samples. The incident X-ray beam (Cu Kα, 40 kV, 25 mA) was passed through a graphite filter and a pulse height discriminator to achieve further monochromatization.

Transmission electron microscopy (TEM)

Samples were cut with a razor blade into small pyramidal shapes and mounted onto block holders with superglue adhesive and allowed to dry overnight. Thin sections were made with a Reichert Ultracut S ultramicrotome with a Cryo-FCS system (Leica, Inc., Deerfield, IL). Sections were cut to 200 nm dry thickness with a 35° cryo-diamond knife (Diatome, Electron Microscopy Sciences, Ft. Washington, PA) and transferred onto 300-hexmesh copper grids. Images were taken with a JEOL 1200 EXII scanning and transmission electron microscope (Japan Electron Optics Laboratory, Peabody, MA) at 80 kV with a Megaview III digital camera and SIS Pro software (Soft Imaging System, Corp., Lakewood, CO) at the Bessey Microscopy Facility, Iowa State University (Ames, IA). Images were taken at magnifications of 100,000 and 250,000× (the corresponding scales for these magnifications were 200 and 100 nm, respectively).

Dynamic mechanical analysis (DMA)

The dynamic mechanical properties of the bulk polymers were determined with a PerkinElmer (Norwalk, CT) dynamic mechanical analyzer (DMA Pyris-7e) in three-point bending mode with a 100-mN static force and a 110-mN dynamic force. We prepared a rectangular specimen by machining the cylindrical product (obtained from heating in a vial) to specimens 2 mm thick and 5 mm deep, and the span-to-depth ratio was maintained at approximately 4. Each specimen was first cooled under liquid nitrogen to approximately −120°C and then heated at 3°C/min at frequency of 1 Hz under helium. The viscoelastic properties, that is, storage modulus, and mechanical loss factor (damping) were recorded as a function of temperature. The glass-transition temperature of the polymer was obtained from the peak of the loss tangent plot. The crosslink density (ν_e) was determined from the rubbery modulus plateau on the basis of the theory of rubber elasticity:[31,32]

$$E' = 3\nu_e RT \quad (1)$$

where E' is the storage modulus (i.e., Young's modulus) of the crosslinked polymer in the plateau region (Pa), R is the universal gas constant (8.314 J mol^{-1} K^{-1}), and T is the absolute temperature (K).

Compressive mechanical testing

Compressive mechanical tests were performed according to the ASTM D 695M-91 specification with an Instron model 4502 universal testing machine (Instron Corp., Canton, MA) at a crosshead speed of 1 mm/min. Cylindrical specimens 10 mm in diameter and 21 mm in height were used for testing. Five specimens were tested for each sample. The moduli of elasticity (Young's modulus) in compression were obtained from the initial slope of the stress–strain curves. The compressive strengths corresponded to the stress at which the cylindrical specimen broke. The ultimate compressive strength and compression at break of the polymers were obtained from the break point of the samples in the compressive tests. The toughness of the polymer, which was the fracture energy per unit volume of the specimen, was obtained from the area under the corresponding compressive stress–strain curve.

Thermogravimetric analysis (TGA)

A PerkinElmer thermogravimetric analyzer (model Pyris 7e) was used to test the thermal stability of the samples. The change in weight loss of the samples was measured by heating in air (20 mL/min) from 30 to 650°C at a programmed rate of 20°C/min.

RESULTS AND DISCUSSION

WAXRD

The WAXRD pattern for the TUNG nanocomposites is shown in Figure 1. The variations of the interlayer distance for the montmorillonite clay before and after treatment with CTAB were found to be 1.496 and 1.801 nm, respectively. The nanocomposites

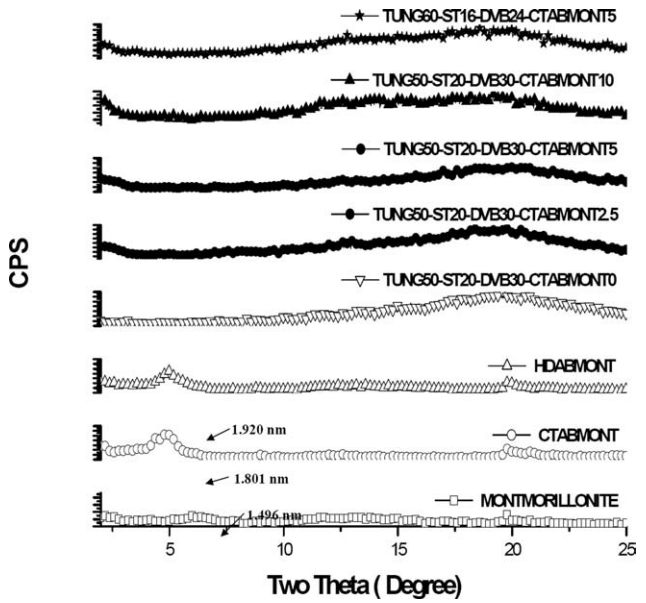

Figure 1 WAXRD patterns of montmorillonite, CTABMONT, HDABMONT, and various TUNG–ST–DVB nanocomposites. CPS, counts per second.

prepared from the modified clays were also studied by WAXRD. A peak in the modified nanoclay was observed at an angle of 5° (2θ). This peak totally vanished in all of the nanocompostes. Park and Jana[33] observed similar results for epoxy nanoclay composites. The vanishing of the clay peak was also observed by Su and Wilkie,[34] Riedl et al.,[35] and Davis et al.[36] According to these authors, the vanishing of the WAXRD peak in the nanocomposite indicated the delamination or exfoliation of the stacked layers of the nanoclay in the polymer nanocomposites. However, Pittman et al.,[37] during their studies on the extent of delamination of clays in polydicyclopentadiene nanocomposites, commented that the XRD results could not be used alone as a criterion for exfoliation. Thus, although the vanishing of the peak due to clays in the nanocomposites (Fig. 1) apparently indicated a distortion of the nanoplaty layers, it could not be used as a confirmatory tool because of the weak signals in WAXRD.

TEM

Figures 2–4 show the TEM images of the synthesized polymer samples. The photograph on the right side is magnified 100,000×, whereas the photograph on the left side is of the same material but at a different magnification of 250,000× (the corresponding scales for these magnifications are 200 and 100 nm, respectively). In all of these photographs, the black area indicates the nanofiller, and the white area corresponds to the polymer matrix.[38] The layered structure of montmorillonite was evident from all of the samples. As evident from Figures 2–4, these platy layers were present in the form of tactoids, showing no exfoliation. It is evident from the images in Figure 2 that the layers were more distinct at lower concentrations of nanofiller. From these results, we assumed that the nanolayers were separated from each other by polymer chains. At higher concentrations of nanofiller, the nanolayers were superimposed on each other, which to their behaving like an ordinary filler (10%). As the concentration of the TUNG increased in the polymer composition for a fixed (5%) dose of nanofiller, the density of the black area increased, which indicated a reduction in the distortion level of the layered structures (Fig. 3). In the case of a sample without any TUNG (S10), less distortion was observed. This was due to very fast crosslinking of the ST and DVB, which provided less

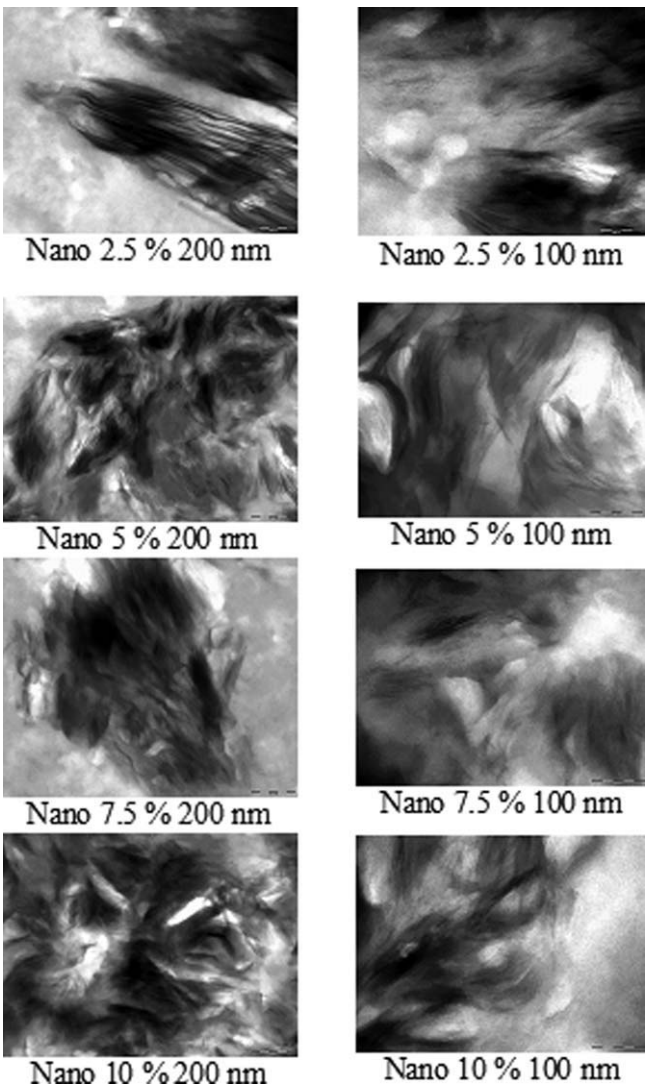

Figure 2 TEM micrographs of nanocomposites of TUNG50–ST20–DVB30 polymers filled with 2.5, 5, 7.5, or 10% CTABMONT (S2, S3, S4, and S5, respectively, in Table I). All these micrographs have been magnified 100,000 and 250,000× (the corresponding scales for these magnifications are 200 and 100 nm, respectively).

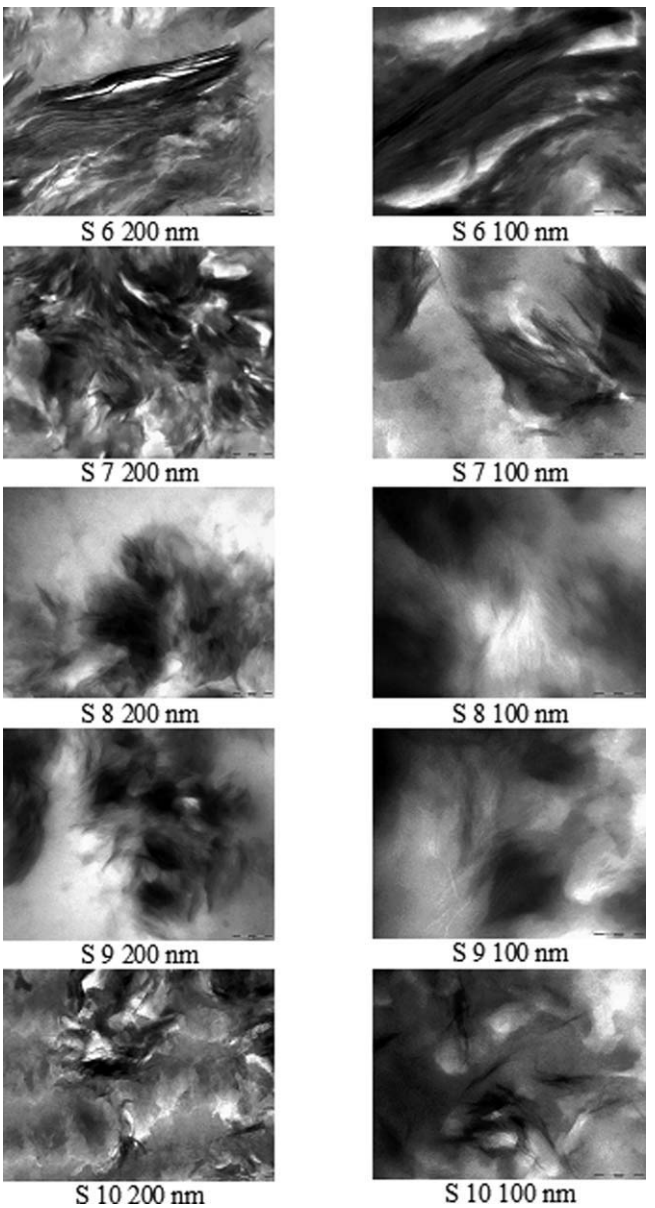

Figure 3 TEM micrographs of nanocomposites with various TUNG contents [30 (S6), 40 (S7), 60 (S8), or 70% (S9) in TUNG–ST–DVB polymers filled with 5% CTABMONT], TUNG (S10), and aromatic nanocomposites with 2.5% CTABMONT (S11). All these micrographs have been magnified 100,000 and 250,000× (the corresponding scales for these magnifications are 200 and 100 nm, respectively).

time for intercalation. On the other hand, samples with a higher oil content, such as S9, were slowly crosslinked, which led to a less crosslinked system. The low crosslink density was unable to exert sufficient force to separate the platy-layered structure, which caused less distortion in polymers containing higher amounts of oil.

Figure 4 shows the TEM micrographs of various nanocomposites. The effect of various parameters, such as the aromatic (S13) and TUNG (S14) intragallery, stirring (S15, S17), and filler modification (S16), on the extent of exfoliation of the nanofiller during *in situ* polymerization are shown in Figure 4. On comparing S13 and S14, we observed that the black shady areas increased in S13 (aromatic intragallery), compared to those in S14 (TUNG intragallery). Because the aromatic intragallery formed at a faster rate, the time for distortion was much less than that for the TUNG intragallery. Thus, in the case of the

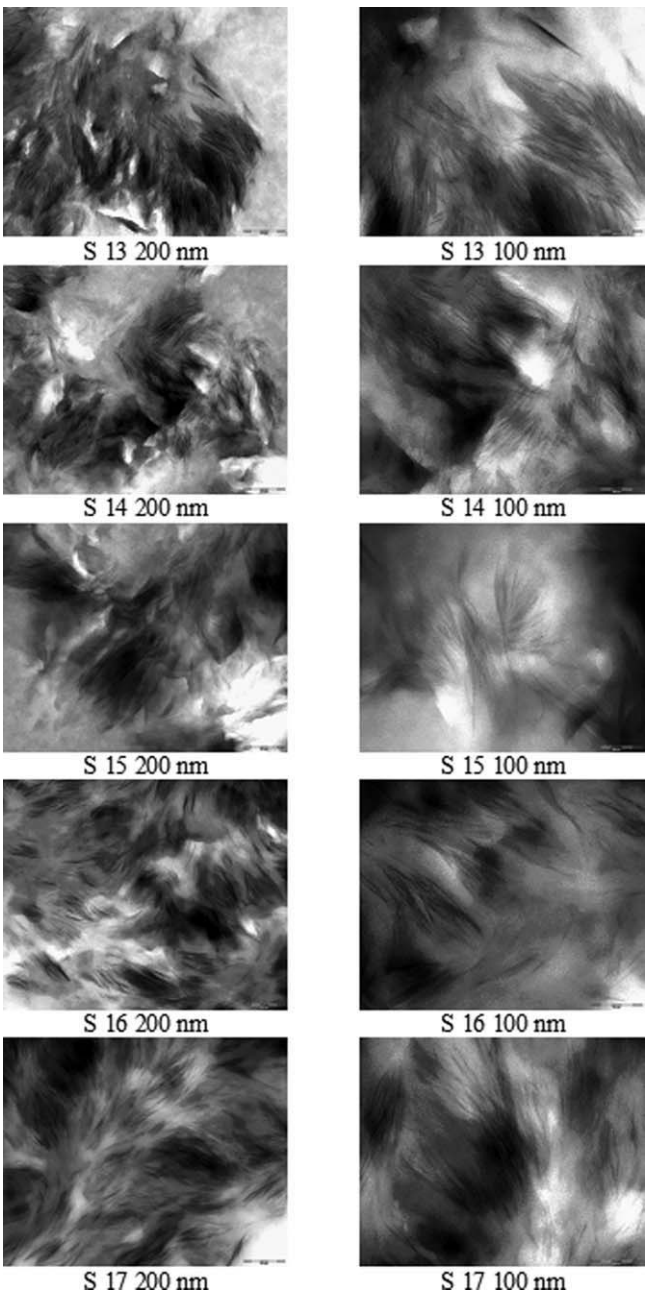

Figure 4 TEM micrographs of nanocomposites of TUNG50–ST20–DVB30 polymers filled with 2.5% HDABMONT (S12) or 2.5% CTABMONT under various mixing conditions (S13–S17 in Table I). All these micrographs have been magnified 100,000 and 250,000× (the corresponding scales for these magnifications are 200 and 100 nm, respectively).

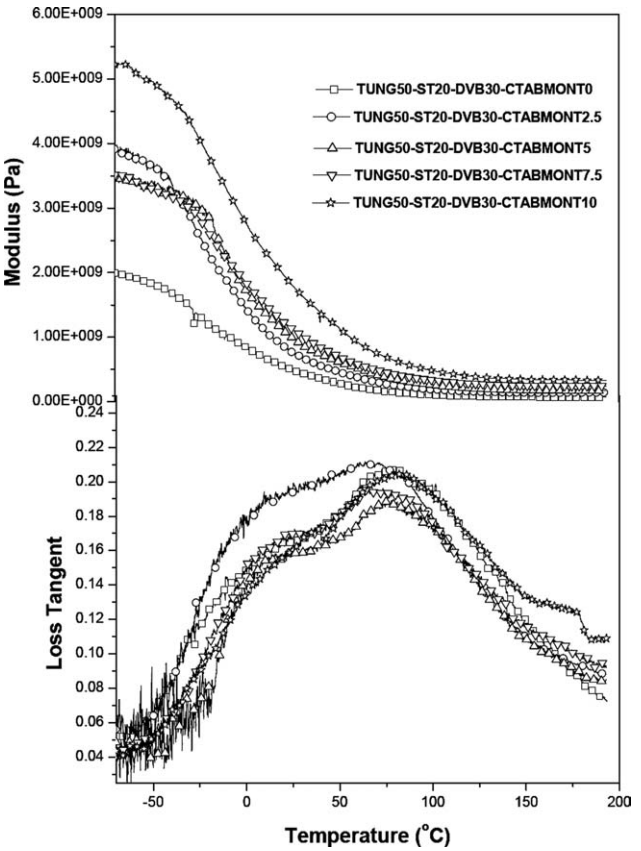

Figure 5 Variation of the storage modulus and loss tangent with the temperature for TUNG50–ST20–DVB30 polymers filled with 0, 2.5, 5, 7.5, or 10% CTABMONT.

TUNG intragallery, the platy layers of the nanofiller were much more distorted. A similar observation was made for S10, shown in Figure 3.

DMA

Figures 5–7 show the variation of the loss tangent and the storage modulus versus the temperature. The glass-transition temperatures obtained from the loss tangent peaks and the crosslink densities calculated from the plateau storage moduli [eq. (1)] are listed in Table II. Figure 5 reports results for the nanocomposites having fixed polymer compositions but various concentrations of the nanofiller. From the loss tangent plots of Figure 5, a broad peak along with a hump in the loss tangent indicated a freezing of the long-range segmental motion of the main chain of the copolymers. This temperature is usually known as the *glass-transition temperature*.[32] The presence of humps indicated the presence of a short oily segment,[31] believed to be grafted onto the main chain.[32] The glass-transition temperature varied from 65.9 to 81.3°C for different percentages of CTAB-modified montmorillonite (CTABMONT) with the same polymer compositions (Table II). At the peak loss tangent temperature (glass-transition temperature), the loss tangent was observed to be at a minimum for the sample with 5% CTABMONT. The broad loss tangent peak in the sample without any nanofiller got sharper upon addition of nanofiller up to a concentration of 5%. The sharpening of the peak and a reduction in the loss tangent value up to 5% nanofiller indicated an increase in the crosslink density caused by a most notable formation of a nanocomposite. The increase in the crosslink density with an increase in nanofiller concentration was believed to be caused by an increase chemical crosslinks between the oil. The thermal polymerization and crosslinking of the TUNG polymers occurred via free-radical polymerization.[31–32] It has already been established that certain cations assist in the thermal polymerization of reactive oils.[39] The presence of residual sodium ions and other ions in the modified montmorillonite may have assisted in the polymerization and crosslinking of TUNG, which led to an increase in the crosslink density. The storage modulus decreased with an increase in the temperature, and there was a catastrophic fall in the modulus around the glass-transition temperature. The modulus of the polymer samples increased with

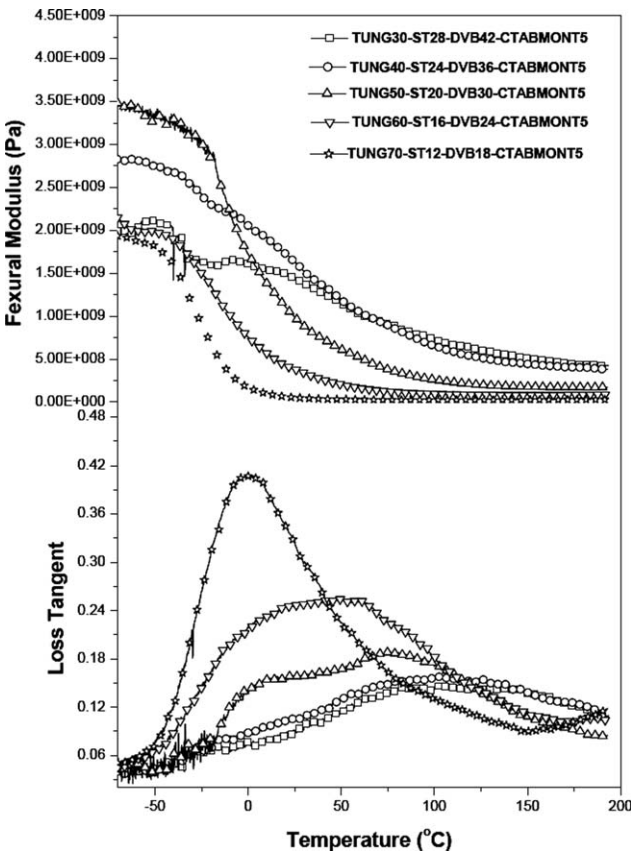

Figure 6 Variation of the storage modulus and loss tangent with the temperature for nanocomposites with various contents of TUNG [30, 40, 50, 60, or 70% in TUNG–ST–DVB polymers filled with a fixed dose (5%) of CTABMONT].

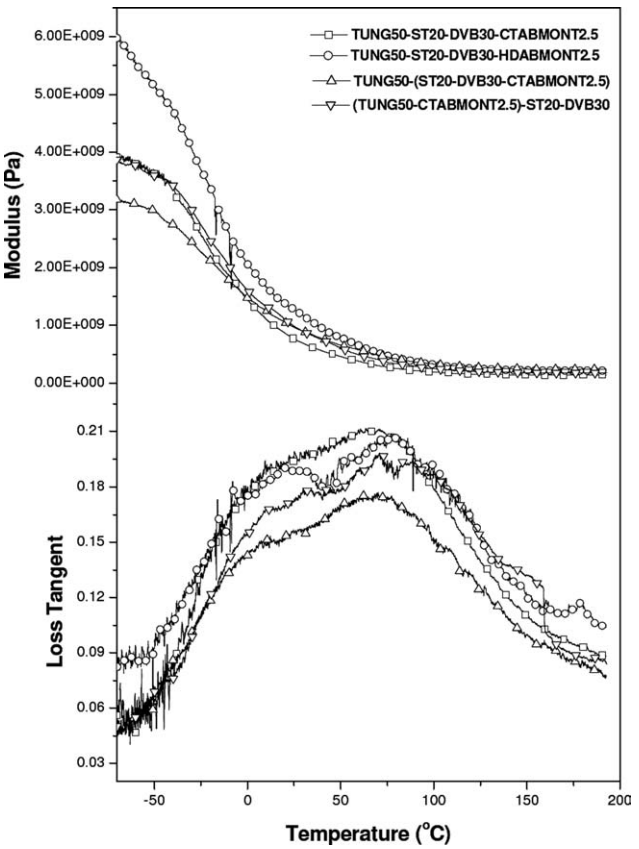

Figure 7 Variation of the storage modulus and loss tangent with the temperature for TUNG50–ST20–DVB30 polymers filled with 2.5% HDABMONT or CTABMONT and 2.5% CTABMONT filled TUNG and aromatic intragalleries.

increasing filler content. The decrease around the glass-transition temperature was the sharpest for the 10% nanofiller, and the decrease was gradual as the filler content decreased. The crosslink densities, as calculated from the storage modulus (Table II), increased with an increase in the nanofiller content in the polymer.

Figure 6 shows the variation in loss tangent and flexural modulus for TUNG samples in which the concentration of the TUNG was varied at a fixed (5%) dose of nanofiller. The loss tangent peak was sharp and narrow for 70% TUNG, and the peak broadened as the concentration of the TUNG in the samples decreased. A hump appeared at lower concentrations of TUNG, and this hump disappeared in the sample with 70% TUNG. However, for the sample with 70% TUNG, the loss tangent started to increase beyond 150°C; this indicated the start of another relaxation process at the higher temperature. The sharp glass transition for the 70%-TUNG-containing sample indicated its rubbery character. Below the glass-transition temperature, the modulus was observed to be at a maximum for 50% TUNG, followed by the 40 and 30% TUNG samples. The highest modulus beyond the glass-transition temperature and the sharp decrease around the glass transition for the sample with 50% TUNG indicated a much better packing of the platy nanolayers of the nanofillers in this particular sample of the polymer at a lower temperature. Above the glass-transition temperature, the modulus value decreased with an increase in the TUNG content. The decrease in the modulus around the glass-transition temperature was sharp for 70% TUNG, and the sharpness diminished with a decrease in the TUNG in the samples. The crosslink densities, as calculated from the storage modulus (Table II), decreased with an increase in the TUNG concentration (at a fixed dose of filler)

TABLE II
Dynamic Mechanical, Mechanical, and Thermal Properties of the TUNG Nanocomposites

	Dynamic mechanical properties		Compressive strength		TGA results (°C)			
Entry	T_g (°C)	v_c (mol/m^3)	E (GPa)	σ_b (MPa)	$T_{5\%}$	$T_{10\%}$	T_{1max}	T_{2max}
S1	77.5	7.0×10^3	0.45	81.3	335	374	481	576
S2	65.9	1.3×10^4	0.53	97.6	342	382	481	582
S3	76.6	1.7×10^4	0.58	110.4	315	358	482	583
S4	65.5	2.4×10^4	0.59	121.0	313	365	461	593
S5	81.3	3.3×10^4	0.60	125.1	283	333	458	588
S6	116.2	4.8×10^4	1.08	121.2	352	377	473	604
S7	102.4	4.2×10^4	0.69	147.5	338	382	497	594
S8	50.7	7.8×10^3	0.33	55.0	326	374	485	588
S9	0.4	2.3×10^3	0.09	15.5	318	371	486	459
S12	76.4	2.1×10^4	0.34	82.4	331	379	488	601
S13	70.9	2.3×10^4	0.58	104.5	342	384	485	583
S14	72.9	1.7×10^4	0.44	94.3	347	389	490	590
S15	—	—	0.35	75.8	—	—	—	—

v_c = crosslink density; E = Young's modulus; σ_b = compressive strength at break; T_{1max} = first-stage degradation temperature; T_{2max} = second-stage degradation temperature; $T_{5\%}$ = temperature at which the 5% weight loss was observed; $T_{10\%}$ = temperature at which the 10% weight loss was observed; T_g = glass-transition temperature.

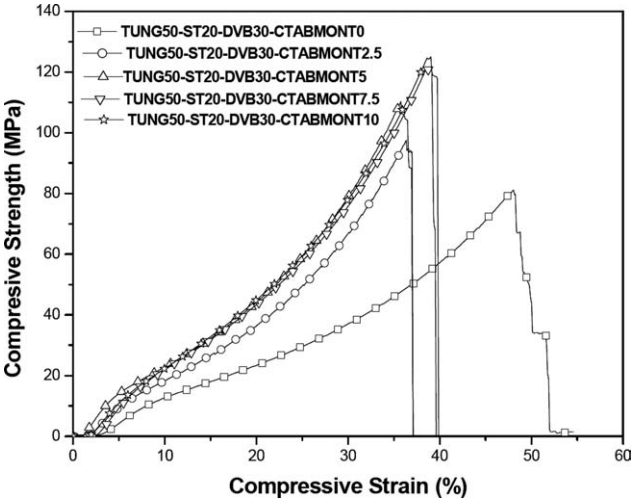

Figure 8 Variation of the compressive strength with the strain for TUNG50–ST20–DVB30 polymers filled with 0, 2.5, 5, 7.5, or 10% CTABMONT.

in the polymer composition. With increasing crosslink density, the number of available chain segments, which imparted chain flexibility, decreased; this caused small polymer chains. The flexible chains showed rubberlike properties, and these imparted a sharpness to the peak. As the chains got shorter, the sharpness of the peaks decreased, and they became broad.

Figure 7 shows the variation in the loss tangent and the flexural modulus with the temperature for samples having the same polymer composition and nanofiller concentration. The variables in these samples were the type of surfactant used for the modification of nanofiller and the sequence of the addition of nanofiller (galleries). The effects of two different modifiers, such as CTAB and HDAB, on the dynamic mechanical properties were compared. The effects of various galleries, such as aromatics and TUNG intragallery and mixed gallery (gallery in both aromatics and TUNG), on the dynamic mechanical properties were also compared. The aromatic intragallery showed the sharpest peak, whereas the peak was broadest for the mixed one. The loss tangent peak maxima (an indicator of damping) for the mixed intragallery was the highest, followed by HDAB, the aromatic intragallery, and the TUNG intragallery. The sample with HDAB-modified montmorillonite (HDABMONT) exhibited a higher modulus than that with CTABMONT. Below the glass-transition temperature, the aromatic intragallery exhibited a lower modulus compared to the sample with a TUNG gallery and a mixed intragallery. Beyond the glass-transition temperature, the TUNG intragallery exhibited a higher modulus than the mixed intragallery. The crosslink densities, as calculated from eq. (1) (Table II), were higher in the aromatic intragallery than in the TUNG intragallery. When the crosslink density of sample 2 was compared with that of sample 12 (see Table II), we observed that the polymer with the same concentration of nanofiller (2.5%) but with different modifiers showed different crosslink densities. Sample 2, with the CTAB-modified filler, exhibited a lower crosslink density compared to sample 12, with the HDAB-modified filler.

Compressive mechanical testing

For many insulation applications (including cryogenic and low-temperature tank bottoms, insulated pipe supports and hangers, underground pipe vessels, parking decks/plazas, roof applications, and docks), superior compressive strength performance is a prerequisite. The compressive mechanical strength of these composite samples has been studied and found to be better than that of the virgin polymers. Figure 8 shows the compressive strengths of the polymers with 0 to 10% nanofiller. The compressive strength was the lowest for the virgin polymer (without nanofiller), and it increased with increasing nanofiller concentration. The toughness (area under the curve) also improved upon the addition of nanofiller. The compressive properties of these polymers are reported in Table II. As in Table II, with an increase in the filler contents, both the Young's modulus and tensile strength increased. The improvement in the mechanical properties (Young's modulus, tensile strength, and toughness) on the addition of filler could be explained by the enhancement of the interaction between the filler and polymer chains at the molecular level (nanolevel). The nanolayers of the filler could place themselves between two polymer chains at the molecular

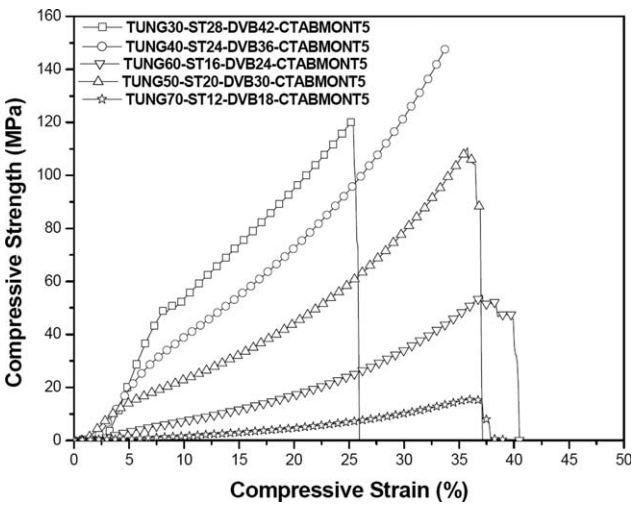

Figure 9 Variation of the compressive strength with the strain for nanocomposites with various contents of TUNG [30, 40, 50, 60, or 70% in TUNG–ST–DVB polymers filled with a fixed dose (5%) of CTABMONT].

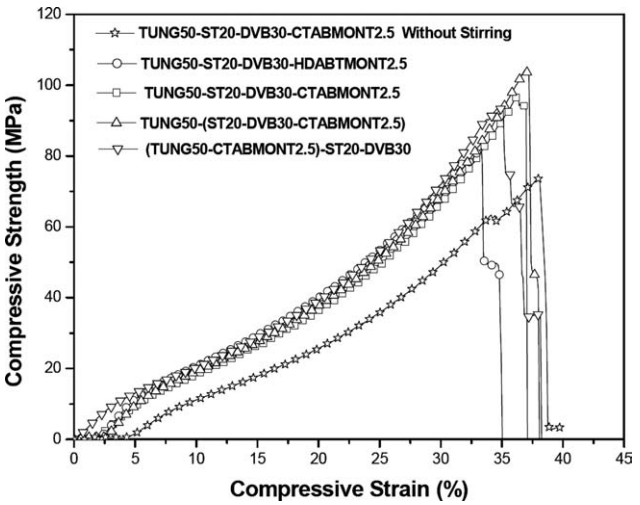

Figure 10 Variation of the compressive strength with the strain for TUNG50–ST20–DVB30 polymers filled with 2.5% HDABMONT or CTABMONT and 2.5% CTABMONT filled TUNG and aromatic intragalleries.

level. Thus, the overall stiffness of the material (nanocomposites) increased, which led to an increase in the mechanical properties. Figure 9 shows the polymer samples with different monomer compositions with the nanofiller level held at 5%. The compressive strength and the toughness increased with an increase in the aromatic concentration in the polymer sample, reaching maxima at 40% TUNG (60% aromatics) and then decreasing with higher aromatics. The Young's modulus also increased with an increase in the aromatic content.

Figure 10 shows the compressive strength of the polymer samples with 2.5% nanofiller. Different methods were adopted during the mixing of the filler with the monomers. The sample without stirring exhibited the lowest strength, Young's modulus, and toughness. The aromatic intragallery exhibited a slightly higher strength, toughness, and Young's modulus compared to the samples with a TUNG intragallery and HDABMONT-filled mixed gallery.

Thus, an overall improvement in the Young's modulus and compressive strength upon incorporation of a nanofiller was observed. The improvement in these properties indicated the presence of a distorted (possibly partially intercalated) platy-layered structure in the nanofiller.

TGA

The thermogravimetric studies of the polymer samples with different percentages of nanofiller are reported in Figure 11. A two-stage degradation was observed for all of the polymer samples. The first-stage degradation was observed around 480°C, and the second-stage degradation was observed around 580°C. In the first-stage degradation, a weight loss of 80–85% was observed. In the second-stage degradation, the virgin polymer (without nanofiller) was burned off completely, whereas the other samples were burned with retention of the filler concentration. The thermogravimetric results for the samples are reported in Table II. The temperatures at which 5 and 10% weight losses were observed to decrease with an increase in nanofiller concentration (for the fixed polymer compositions) and TUNG concentration (for fixed filler doses). The first-stage degradation temperature decreased with an increase in filler content (for the fixed polymer composition). However, the second-stage degradation temperature remained almost unaltered when the polymer composition or filler concentration was changed.

CONCLUSIONS

Novel nanocomposites were prepared by the *in situ* thermal copolymerization of TUNG–ST–DVB in the presence of organically modified montmorillonite. The synthesized nanocomposites were characterized by XRD, TEM, DMA, and their mechanical properties. The XRD results indicate distortion of the platy nanolayers of nanofiller in the composite. All of these nanocomposites exhibited a distorted platy-nanolayered structure in the form of tactoids under a transmission electron microscope. Depending on the concentration of nanofiller and TUNG–ST–DVB polymer in the nanocomposite, a variation in the level of distortion was observed by TEM. A broadened glass-transition temperature along with a hump (from DMA) of the nanofilled polymers indicated the presence of a majority constituent consisting of TUNG and aromatics, along with grafted TUNG. The improvement in the Young's modulus and compressive strength upon the incorporation of a nanofiller

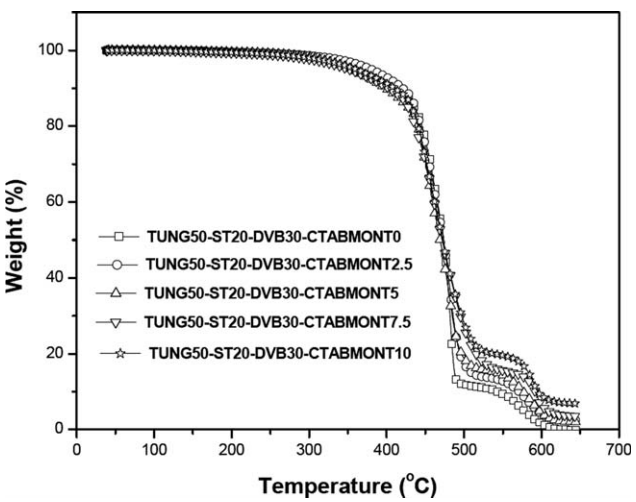

Figure 11 Variation of the weight loss with the temperature for TUNG50–ST20–DVB30 polymers filled with 0, 2.5, 5, 7.5, or 10% CTABMONT.

indicated the presence of a distorted (possibly partially intercalated) structure for the nanofiller. However, from all of these studies, it was not possible to estimate the exact level of delamination/distortion in these TUNG–ST–DVB nanocomoposites.

References

1. Pinnavaia, T. J.; Beall, G. W. Polymer–Clay Nanocomposites; Wiley: New York, 2000.
2. Vaia, R. A.; Ishii, H.; Giannelis, E. P. Chem Mater 1993, 5, 1694.
3. Ho, R. M.; Chen, S. Z. D.; Hsiao, B. S.; Gardner, K. H. Macromolecules 1994, 27, 2136.
4. Zhao, Y. X. Clay Minerals; Geological Press of China: Beijing, 1980.
5. Clarey, M.; Edwards, J.; Tsipursky, S. J.; Beall, G. W.; Eisenhour, D. D. U.S. Pat.6,050,509 (2000).
6. Nanoparticles: From Theory to Application; Schmid, G., Ed.; Wiley-VCH: Weinheim, 2004.
7. Ding, Y.; Jones, D. J.; Maireles-Torres, P.; Roziere, J. Chem Mater 1995, 7, 562.
8. Peng, X.; Wickham, J.; Alivisatos, A. P. J Am Chem Soc 1998, 120, 5343.
9. Kaempfer, D.; Thomann, R.; Mulhaupt, R. Polymer 2002, 43, 2909.
10. Beecroft, L. L.; Ober, C. K. Chem Mater 1999, 11, 1302.
11. Nazar, L. F.; Zhang, Z.; Zinkweg, D. J Am Chem Soc 1992, 114, 6239.
12. Robeson, L. M. J Membr Sci 1991, 62, 165.
13. Routkevitch, D.; Tager, A. A.; Haruyama, J.; Al-Mawlawi, D.; Moskovits, M.; Xu, J. M. IEEE Trans Electron Dev 1996, 43, 1646.
14. Cao, G.; Garcia, M. E.; Aleala, M.; Burgess, L. F.; Mallouk, T. E. J Am Chem Soc 1992, 114, 7574.
15. Uyama, H.; Kuwabara, M.; Tsujimoto, T.; Nakano, M.; Usuki, A.; Kobayashi, S. Chem Mater 2003, 15, 2492.
16. Saminathan, K.; Selvakumar, P.; Bhatnagar, N. Polym Test 2008, 27, 296.
17. Wilkinson, A. N.; Man, Z.; Stanford, J. L.; Matikainen, P.; Clemens, M. N.; Lees, G. C.; Liauw, C. M. Compos Sci Technol 2007, 67, 3360.
18. Drown, E. K.; Mohanty, A. K.; Parulekar, Y.; Hasija, H.; Harte, B. R.; Misra, M.; Kurian, J. V. Compos Sci Technol 2007, 67, 3168.
19. Bergaya, F. A. Microporous Mesoporous Mater 2008, 107, 141.
20. Xue, S.; Pinnavaia, T. J. Microporous Mesoporous Mater 2008, 107, 134.
21. Ding, Y.; Zhang, X.; Xiong, R.; Wu, S.; Zha, M.; Tang, H. Eur Polym J 2008, 44, 24.
22. Lagaly, G. Solid State Ionics 1986, 22, 43.
23. Crystal Structure of Clay Minerals and Their X-Ray Identification; Brindley, G.; Brown, G., Eds.; Mineral Society: London, 1980; p 227.
24. De Carvalho, A. J. F.; Curvelo, A. A. S.; Agnelli, J. A. M. Carbohydr Polym 2001, 45, 189.
25. Viville, P.; Lazzaroni, R.; Pollet, E.; Alexandre, M.; Dubois, P.; Borcia, G.; Pireaux, J. J. Langmuir 2003, 19, 9425.
26. Agag, T.; Koga, T.; Takeichi, T. Polymer 2001, 42, 3399.
27. Chen, T. K.; Tien, Y. I.; We, K. H. J Polym Sci Part A: Polym Chem 1999, 37, 2225.
28. Suh, D. J.; Lim, Y. T.; Park, O. O. Polymer 2000, 41, 8557.
29. Chen, G.; Liu, S.; Chen, S.; Qi, Z. Chem Phys 2001, 202, 1189.
30. Lee, J. W.; Lim, Y. T.; Park, O. O. Polym Bull 2000, 45, 191.
31. Li, F.; Larock, R. C. Biomacromolecules 2003, 4, 1018.
32. Kundu, P. P.; Larock, R. C. Biomacromolecules 2005, 6, 797.
33. Park, H. J.; Jana, S. C. Macromolecules 2003, 36, 2758.
34. Su, S.; Wilkie, C. A. J Polym Sci Part A: Polym Chem 2003, 41, 1124.
35. Feng, W.; Ait-Kadi, A.; Riedl, B. Macromol Rapid Commun 2002, 23, 703.
36. Davis, C. H.; Mathias, L. J.; Gilman, J. W.; Schiraldi, D. A.; Shields, J. R.; Trulove, P.; Sutto, T. E.; Delong, H. C. J Polym Sci Part B: Polym Phys 2002, 40, 2661.
37. Yoonessi, M.; Toghiani, H.; Kingery, W. L.; Pittman, C. U., Jr. Macromolecules 2004, 37, 2511.
38. Hasegawa, N.; Usuki, A. Polym Bull 2003, 51, 77.
39. Kundu, P. P.Larock, R. C. Prog Org Coat 2009, 65, 10.